Power Optimization for Photovoltaic Microconverters Using Multivariable Newton-Based Extremum Seeking

Azad Ghaffari, Miroslav Krstić, *Fellow, IEEE*, and Sridhar Seshagiri

***Abstract*— Extremum seeking (ES) is a real-time optimization technique that has been applied to maximum power point tracking (MPPT) design for photovoltaic (PV) microconverter systems, where each PV module is coupled with its own dc/dc converter. Most of the existing MPPT designs are scalar, i.e., employ one MPPT loop around each converter, and all designs, whether scalar or mutivariable, are gradient based. The convergence rate of gradient-based designs depends on the Hessian, which in turn is dependent on environmental conditions, such as irradiance and temperature. Therefore, when applied to large PV arrays, the variability in environmental conditions and/or PV module degradation results in nonuniform transients in the convergence to the maximum power point (MPP). Using a multivariable gradient-based ES algorithm for the entire system instead of a scalar one for each PV module, while decreasing the sensitivity to the Hessian, does not eliminate this dependence. We present a recently developed Newton-based ES algorithm that simultaneously employs estimates of the gradient and Hessian in the peak power tracking. The convergence rate of such a design to the MPP is independent of the Hessian, with tunable transient performance that is independent of environmental conditions. We present simulation as well as the experimental results that show the effectiveness of the proposed algorithm in comparison with the existing scalar designs, and also to multivariable gradient-based ES.**

***Index Terms*— Dc/dc microconverters, maximum power point tracking (MPPT), Newton-based extremum seeking (ES), photovoltaic (PV) arrays.**

I. Introduction

MAXIMUM power point tracking (MPPT) algorithms for extracting the maximum achievable power from a photovoltaic (PV) system have been studied by several researchers [4], [15], [17]–[19], with detailed comparisons presented in [5], [11], and [12]. Several recent works [2], [3], [14], [16] have focused on the application of gradient-based extremum seeking (ES) [1] to MPPT design.

To the best of our knowledge, there are a limited number of multivariable MPPT schemes described in the literature, among which we refer the reader to [15], [18], and [19]. Reference [19] uses a multivariable version of the popular Perturb and Observe (P&O) algorithm. Unlike scalar designs that require one current sensor for each module, the algorithm only requires a single current sensor on the dc bus. The operating point of the dc/dc converters is perturbed asynchronously, to minimize the possibility of converter interaction having a detrimental effect on the other modules. Closely related to [19] is the work in [18], where extra variables are employed in the classical P&O algorithm to overcome the limitation of scalar designs, which the authors say fail when the feasibility region is nonconvex. It is unclear how [18] compares with distributed architectures, with respect to power loss recovery in the case of module mismatch. Reference [15] uses particle swarm optimization (PSO), which is an algorithm that employs multiple agents to search for the peak power. This paper does not describe the specific criteria used to select the number of agents and parameters of the PSO, nor the conditions on the voltage and power boundary limits to stop the algorithm at maximum power point (MPP). In addition, in a PV system with a higher number of PV modules, the process of reinitialization and the tracking performance depend strongly on variable conditions, such as environmental factors, the nature of the PV modules, and the shading area. The authors claim that the required number of sensors is reduced to two, but to compute the pulse duration, the output voltage of each boost converter needs to be monitored by a separate sensor. The method also has an adaptation time of the order of 1–2 s. By contrast, the response time in ES-based designs is much smaller, of the order of 0.1 s.

Expansion of the conventional P&O MPPT methods to the case of cascade PV modules with microconverters (one dc/dc converter for each module), as presented in [19], requires a step-by-step P&O, namely the core part of the algorithm is a scalar P&O, which finds the MPP of each PV module at a time. This results in a longer convergence time. Furthermore, coupling effects between modules that are exacerbated due to a partial shading and model mismatch cause nonuniform transient responses under different environmental conditions. This problem holds in the PSO method of [15]. Multivariable ES, unlike the other MPPT approaches, treats the entire cascade PV system as a whole and it simply fits every PV system architecture without any need to redesign the control loop.

In [9] and [10], we presented a multivariable gradient-based ES MPPT design for the microconverter architecture, where

Manuscript received June 3, 2013; revised October 4, 2013; accepted January 3, 2014. Manuscript received in final form January 15, 2014. Date of publication February 17, 2014; date of current version October 15, 2014. Recommended by Associate Editor M. Guay.

A. Ghaffari and M. Krstić are with the Department of Mechanical and Aerospace Engineering, University of California, San Diego, La Jolla, CA 92093-0411 USA (e-mail: aghaffari@ucsd.edu; krstic@ucsd.edu).

S. Seshagiri is with the Department of Electrical and Computer Engineering, San Diego State University, San Diego, CA 92182-1309 USA (e-mail: seshagir@engineering.sdsu.edu).

Color versions of one or more of the figures in this paper are available online at http://ieeexplore.ieee.org.

Digital Object Identifier 10.1109/TCST.2014.2301172

each PV module is coupled with its own dc/dc converter. The design reduced the number of required sensors (hardware reduction), and was shown to result in more uniform transients under sudden changes in solar irradiance and environmental temperature in comparison with a scalar gradient-based ES for each PV module. However, as is true of gradient-based designs, the convergence to MPP was dependent on the unknown Hessian, and varied with irradiance, temperature, and module degradation and mismatch.

To alleviate the issue of unknown Hessian-dependent convergence of a gradient-based ES algorithm, we presented a multivariable Newton-based ES design for general nonlinear systems in [6]. In comparison with the standard gradient-based multivariable ES, the algorithm in [6] removes the dependence of the convergence rate on the unknown Hessian and makes the convergence rate of the parameter estimates user assignable. In particular, all the parameters can be designed to converge with the same speed, yielding straight trajectories to the extremum even with maps that have highly elongated level sets. When applied to the MPPT problem in PV systems, the method offers the benefit of uniform convergence behavior under a wide range of working conditions, which includes temperature and irradiance variations, and the nonsymmetric power generation of the neighboring PV modules as a result of module degradation or mismatch. Preliminary results were presented in [7].

In this expanded version of [7], we provide detailed guidelines for selection of the ES controller parameters, particularly the frequency distribution of the probing frequencies and bandpass frequencies of the low-pass filters. In addition, while the design was only validated by simulation in [7], here we present experimental results that demonstrate the effectiveness of the proposed algorithm against large step solar irradiance perturbations. Unlike several existing MPPT algorithms, ES requires no programming, and consists essentially of two filters, an oscillator, a multiplier, and an adder, all of which can be implemented using analog hardware (op-amps, resistors, and capacitors). However, as is common in rapid prototyping, our implementation is done using the single-board dSPACE microcontroller.

The rest of this paper is organized as follows. The mathematical model of a PV module, along with a discussion of the dc/dc converter power electronics, is briefly presented in Section II. This section is based on our previous work, and is reproduced here for the sake of completeness/clarity. Section III summarizes the multivariable gradient-based ES scheme in [9] and [10], and allows us to present key distinctions with the proposed design. Our proposed multivariable Newton-based ES is presented and discussed in Section IV. The simulation and experimental results are presented in Section V, and our work is summarized and some concluding remarks made in Section VI.

II. PV Modules and Power Extraction

A. PV Cell Module

Our design and analysis are based on the standard PV cell model described, for example, in [20], and shown schematically in Fig. 1. The PV cell is modeled as an ideal current source of value i_s in parallel with an ideal diode with voltage v_d. Electrical losses and contactor resistance are accounted for by the inclusion of the parallel and series resistances R_s and R_p, respectively. The amount of generated current i_s is dependent on the solar irradiance S and the temperature T through the following equation:

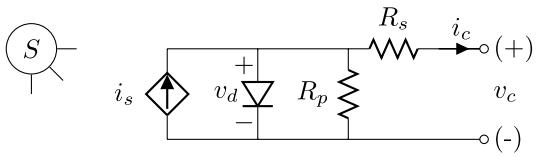

Fig. 1. Equivalent circuit of a PV cell.

$$i_s = (I_s + k_i(T - T_r))\left(\frac{S}{1000}\right) \tag{1}$$

where I_s is a reference short-circuit current, T_r a reference temperature, and k_i the short-circuit temperature coefficient. The diode models the effect of the semiconductor material and its $I-V$ characteristics are given by

$$i_d = i_0\left(\exp\left(\frac{v_d}{\mathrm{N}V_t}\right) - 1\right) \tag{2}$$

$$i_0 = I_0\left(\frac{T}{T_r}\right)^3 \exp\left[\frac{E_g}{\mathrm{N}V_t}\left(\frac{T}{T_r} - 1\right)\right], \quad V_t = \left(\frac{kT}{q}\right) \tag{3}$$

where I_0, E_g, and N are, respectively, the diode reference reverse saturation current, the semiconductor bandgap voltage (barrier height), and the emission coefficient, all three being cell material/construction dependent, V_t is the thermal cell voltage, and $k = 1.38 \times 10^{-23}$ J/K and $q = 1.6 \times 10^{-19}$ C are Boltzman's constant and the charge on an electron, respectively. The cell model described by the above equations along with KCL/KVL: $i_c = i_s - i_d - v_d/R_p$, $v_d = v_c + i_c R_s$, is then scaled to represent a PV module by considering n_s cells in series (each having thermal voltage V_t), so that the terminal $I-V$ relationship for the PV module is given by

$$i = i_s - i_0\left[\exp\left(\frac{\frac{v}{n_s} + i R_s}{\mathrm{N}V_t}\right) - 1\right] - \left[\frac{(\frac{v}{n_s} + i R_s)}{R_p}\right]. \tag{4}$$

For the sake of model development and performing simulations, we pick the PV module 215N from Sanyo, with the following numerical values derived from the manufacturer's datasheet [8]: $E_g = 1.16$ eV, $N = 1.81$, $I_0 = 1.13 \times 10^{-6}$ A, $I_s = 5.61$ A, $k_i = 1.96$ mA/K, $T_r = 298.15$ K, $R_s = 2.48$ mΩ, $R_p = 8.7$ Ω, and the number of PV cells connected in series is $n_s = 72$. The resulting $I-V$ and $P-V$ curves are shown in Fig. 2.

B. Power Electronics

As it is clear from Fig. 2(b) and (d), the power–voltage ($P-V$) characteristic has a unique but (T, S)-dependent peak (v^*, p^*). It is the job of the MPPT algorithm to automatically track this peak. In many grid-tied PV systems (including our current work), this is done by means of a separate dc/dc power electronics stage that serves two functions: 1) regulating the

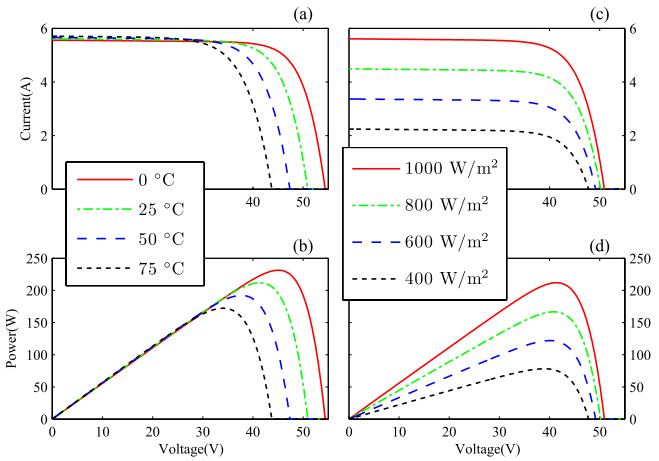

Fig. 2. Characteristic (a) $I-V$ and (b) $P-V$ for varying temperature, $S = 1000$ W/m^2. Characteristic (c) $I-V$ and (d) $P-V$ for varying irradiance, $T = 25$ °C, PV module 215N from Sanyo.

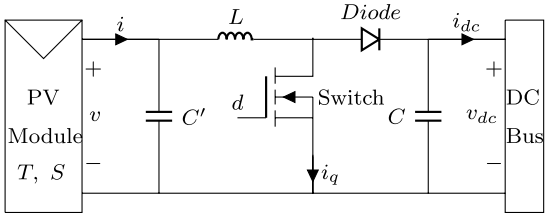

Fig. 3. Dc/dc boost converter for PV module supplying power to dc bus.

output dc voltage at a (near) constant value and 2) extracting maximum power by forcing the PV module output v to equal v^*. Fig. 3 shows this setup for a dc/dc boost converter stage, whose output voltage is maintained constant as $v_{\rm dc}$. The ratio between the input voltage v and output voltage $v_{\rm dc}$ can be controlled by changing the duty cycle of the transistor switch, which serves as the control input d. Under the assumption that the boost converter is working in continuous current mode, and that the switching pulsewidth modulation (PWM) frequency f_c is significantly higher than the bandwidth of the control loop, the boost converter input–output voltage relationship is given by the following (averaged) relations:

$$v = (1-d)v_{\rm dc} \tag{5}$$

$$i_{\rm dc} = (1-d)i. \tag{6}$$

From (4), (5), and Fig. 2(b) and (d), it follows that at the MPP $(v^*,\ p^*)$, the power $p = iv = f(v)v \stackrel{\rm def}{=} J(v)$ satisfies

$$g = \frac{\partial J}{\partial v}(v^*) = 0 \tag{7}$$

$$h = \frac{\partial^2 J}{\partial v^2}(v^*) < 0. \tag{8}$$

In addition, we have $\partial v/\partial d = -v_{\rm dc}$, then

$$\bar{g} = \frac{\partial J}{\partial d}(d^*) = -g v_{\rm dc} = 0 \tag{9}$$

$$\bar{h} = \frac{\partial^2 J}{\partial d^2}(d^*) = h v_{\rm dc}^2 < 0. \tag{10}$$

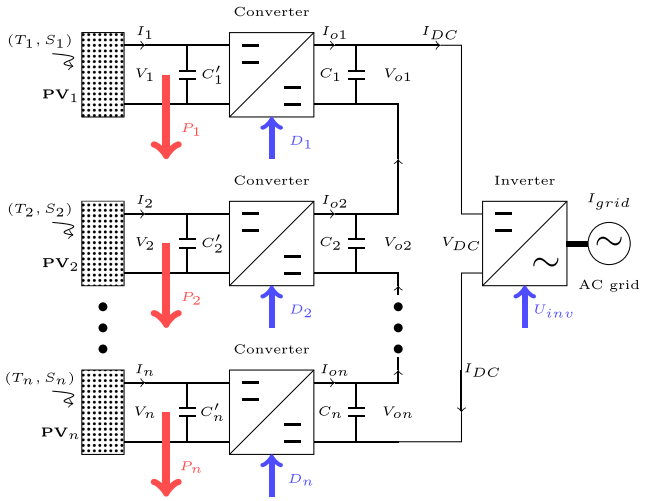

Fig. 4. Cascade PV system including n PV module. Each module has a separate dc/dc converter.

Many MPPT techniques, including the classical P&O class of methods, and ES techniques, are based on detecting the sign of the power gradient.

C. Microconverter Architecture

The above MPPT techniques have been applied to the case of PV modules connected in various series/parallel configurations to form large PV arrays. Traditionally, PV arrays have been connected to the ac power grid through centralized dc/ac power converters (or inverters). These are now giving way to distributed architectures that connect each module to a dedicated converter/inverter. The microconverter configuration, where each PV module is connected to its own dc/dc converter, is the focus of this paper, and is shown schematically in Fig. 4.

A cascade PV system is shown in Fig. 4. A dc/dc boost converter is assigned to each PV module to extract maximum power from the PV system. The output side of the converters is connected in series. The PV system is connected to the power grid through a dc/ac inverter, which has its separate controller. It is assumed that the dc voltage at the input side of the inverter is held constant at $V_{\rm dc}$. Assume that the voltage and current ripple at the output side of converters are negligible. Applying electrical rules on the input side of the inverter gives

$$\sum_{j=1}^{n} V_{\rm oj} = V_{\rm dc} \tag{11}$$

$$I_{\rm oj} = I_{\rm dc} \quad \forall j \in \{1, 2, \ldots, n\}. \tag{12}$$

From (5), (6), and the I–V functional dependence $I_j = f_j(V_j)$, the relation between the voltage $V = [V_1\ V_2\ \cdots\ V_n]^T$ of PV modules and the pulse duration $D = [D_1\ D_2\ \cdots\ D_n]^T$ is defined by n independent equations

$$\sum_{j=1}^{n} \frac{V_j}{1-D_j} = V_{\rm dc} \tag{13}$$

$$(1-D_j) f_j(V_j) = I_{\rm dc} \quad \forall j \in \{1, 2, \ldots, n\}. \tag{14}$$

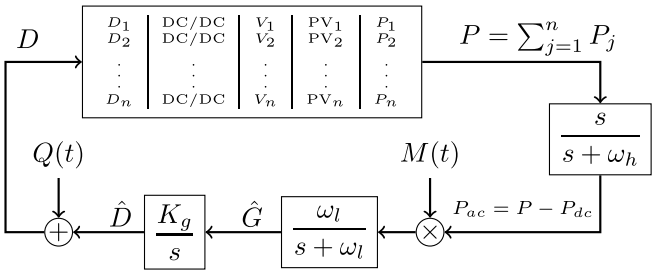

Fig. 5. Multivariable gradient-based ES for MPPT of a PV system.

This means that for each set of pulse duration, we have a unique set of voltages for PV modules. Assuming lossless converters results in $P_{\rm oj} = V_{\rm oj} I_{\rm oj} = P_j$ for all $j \in \{1, 2, \ldots, n\}$. Using (12), we obtain

$$V_{\rm oj} = \frac{P_j}{\sum_{i=1}^{n} P_i} V_{\rm dc} \tag{15}$$

which means that the share of the output voltage of each converter from dc bus voltage is defined by the generated power of its relevant PV module.

We want to maximize the power generated by all PV modules, which is equal

$$P = \sum_{i=1}^{n} P_i = V_{\rm dc} I_{\rm dc}. \tag{16}$$

The following observation is valid about the power.

Assumption 1: From (13)–(16), it follows that there exists $D^* \in \mathbb{R}^n$ such that:

$$\frac{\partial P}{\partial D}(D^*) = 0 \tag{17}$$

$$\frac{\partial^2 P}{\partial D^2}(D^*) = H < 0, \qquad H = H^T. \tag{18}$$

The next section discusses gradient-based ES for the microconverter architecture in Fig. 4, and is extracted from [9] and [10].

III. Multivariable Gradient-Based ES

Fig. 5 shows the multivariable gradient-based ES design, where K_g is a positive diagonal matrix, and the perturbation signals are defined as

$$Q(t) = a[\,\sin(\omega_1 t) \quad \cdots \quad \sin(\omega_n t)\,]^T \tag{19}$$

$$M(t) = \frac{2}{a}[\,\sin(\omega_1 t) \quad \cdots \quad \sin(\omega_n t)\,]^T \tag{20}$$

where ω_j/ω_k are rational for all j and k, and a is a real number, with the frequencies chosen such that $\omega_j \neq \omega_k$ and $\omega_j + \omega_k \neq \omega_m$ for distinct j, k, and m.

In particular, the design derives an estimate $\hat{G}$ of the gradient vector by adding the probing signal Q to the estimate $\hat{D} = [\hat{D}_1 \ \hat{D}_2 \ \cdots \ \hat{D}_n]^T$ of the pulse duration vector (of all the dc/dc converters). With no additional information on the Hessian (and also for simplicity), we choose the amplitudes of the probing signals to all be the same value a. Smallness of the probing frequencies and the matrix gain K_g are ensured by selecting these as

$$\omega_j = \omega\lambda_j, \quad j \in \{1, 2, \ldots, n\} \tag{21}$$

$$\omega_h = \omega\delta\lambda_h \tag{22}$$

$$\omega_l = \omega\delta\lambda_l \tag{23}$$

$$K_g = \omega\delta\kappa_g \tag{24}$$

where ω and δ are small positive constants, and λ_j, λ_h, λ_l, and elements of κ_g are $O(1)$ positive real parameters. It can be shown that for sufficiently small ω, δ, and a, and with $K_g > 0$, the estimate $\hat{D}$ of the pulse duration vector and the output P converge to $O(\omega + \delta + a)$ neighborhoods of the optimal pulse duration $D^* = [D_1^* \ D_2^* \ \cdots \ D_n^*]^T$ and the peak power $P(D^*)$, respectively.

Applying Taylor series expansion to $P(D, t)$ at its maximum point, and noting that $D = D^* + \tilde{D} + Q(t)$, we have

$$P = P^* + \frac{1}{2}(\tilde{D} + Q(t))^T H (\tilde{D} + Q(t)) + R(\tilde{D} + Q(t)) \tag{25}$$

where $\partial P(D^*)/\partial D = 0$ and $R(\tilde{D} + Q(t))$ stands for higher order terms in $\tilde{D} + Q(t)$. We separate (25) into its averaged/dc part $P_{\rm dc}$ and oscillatory/ac part $P_{\rm ac}$ as follows:

$$P = P_{\rm dc} + P_{\rm ac} \tag{26}$$

where

$$P_{\rm dc} = P^* + \frac{1}{2}\tilde{D}^T H \tilde{D} + R_{\rm dc}(\tilde{D}) \tag{27}$$

$$P_{\rm ac} = Q^T(t) H \tilde{D} + \frac{1}{2} Q^T(t) H Q(t) + R_{\rm ac}(\tilde{D} + Q(t)) \tag{28}$$

where $R_{\rm dc}(\tilde{D})$ and $R_{\rm ac}(\tilde{D} + Q(t))$ are higher order dc and ac terms, respectively. The high-pass filter attenuates the averaged/dc part of the power signal while keeps the high-frequency part. Denoting

$$M(t) Q^T(t) = I_{n\times n} + Z_{n\times n} \tag{29}$$

where

$$Z_{jj} = -\cos(2\omega_j t) \tag{30}$$

$$Z_{jk} = \cos((\omega_j - \omega_k)t) - \cos((\omega_j + \omega_k)t), \quad j \neq k \tag{31}$$

we obtain

$$M(t) P_{\rm ac} = H\tilde{D} + ZH\tilde{D} + O(a) \tag{32}$$

where $O(a)$ contains terms of the order of a. From (25), we know that the gradient vector of the cost function is $G = \partial P/\partial \tilde{D} = H\tilde{D}$. Hence, the averaged/dc part of the multiplication of $M(t)$ and $P_{\rm ac}$, which equals to $H\tilde{D}$, is the estimate of the gradient vector of the cost function. An appropriate selection of the low-pass filter removes the oscillatory part of $M(t)P_{\rm ac}$. Regardless of the vector length, n, the same low-pass filter on every channel of the gradient vector guarantees the averaging process and proper attenuation of the high-frequency terms. Referring to (30)–(32), it is clear that the main harmonics in the estimate of the gradient vector

are $2\omega_j$, $\omega_j \pm \omega_k$ for all distinct j and k. This observation motivates the following restriction on the choice of the low-pass filter frequency:

$$\omega_l \ll \{|\omega_j - \omega_k|\} \qquad \forall j \neq k. \tag{33}$$

The linearized update equation for the estimation error $\tilde{D} = \hat{D} - D^*$ is

$$\dot{\tilde{D}} = K_g H \tilde{D}, \quad H := \frac{\partial^2 P}{\partial D^2}(D^*) \tag{34}$$

where H is the Hessian of $P = \sum_{j=1}^{n} P_j$ with respect to the pulse duration vector, D. Our analytical results for the multivariable gradient-based ES design are summarized in the theorem below, the proof of which follows from [13].

Theorem 1: For the system in Fig. 5, under Assumption 1, there exist $\bar{\delta}, \bar{a} > 0$, and for any $|a| \in (0, \bar{a})$ and $\delta \in (0, \bar{\delta})$, there exists $\bar{\omega} > 0$ such that for any given a and δ and any $\omega \in (0, \bar{\omega})$, there exists a neighborhood of the point $(\hat{D}, \hat{G}, P_{\rm dc}) = (D^*, 0, P(D^*))$ such that any solution of the gradient-based ES from the neighborhood exponentially converges to an $O(\omega + \delta + |a|)$ neighborhood of that point. Furthermore, $P(D, t)$ converges to an $O(\omega + \delta + |a|)$ neighborhood of $P(D^*)$.

Since the cost function P varies with irradiance, temperature, and degradation of the PV modules, so does H, and therefore a fixed adaptation gain K_g results in different (condition dependent) convergence rates for each converter. To alleviate the issue of unknown Hessian-dependent convergence, we present in the next section a modified version of a multivariable Newton-based ES design that we developed in [6]. In comparison with the gradient-based design of this section, the Newton-based algorithm makes the convergence rate of the parameter estimates user assignable. In particular, all the parameters can be designed to converge with the same speed, yielding straight trajectories to the extremum even with maps that have highly elongated level sets. When applied to the MPPT problem in PV systems, the method offers the benefit of uniform convergence behavior under a wide range of working conditions that include temperature and irradiance variations, and the nonsymmetric power generation of the neighboring PV modules as a result of module degradation or mismatch.

IV. Multivariable Newton-Based ES

The multivariable Newton-based ES that we propose is shown schematically in Fig. 6. As it is clear from this figure, the proposed scheme extends the gradient-based ES with the estimate $\hat{H}$ of the Hessian. The perturbation matrix $W(t)$ is defined as follows:

$$W_{jj} = \frac{16}{a^2}\left(\sin^2(\omega_j t) - \frac{1}{2}\right) \tag{35}$$

$$W_{jk} = \frac{4}{a^2}\sin(\omega_j t)\sin(\omega_k t), \quad j \neq k \tag{36}$$

where $j, k \in \{1, 2, \ldots, n\}$. The product of $W(t)$ and $P_{\rm ac}$ generates an initial estimate of the Hessian

$$W(t)P_{\rm ac} = \frac{1}{2}WQ^T HQ + WQ^T H\tilde{D} + O(a) \tag{37}$$

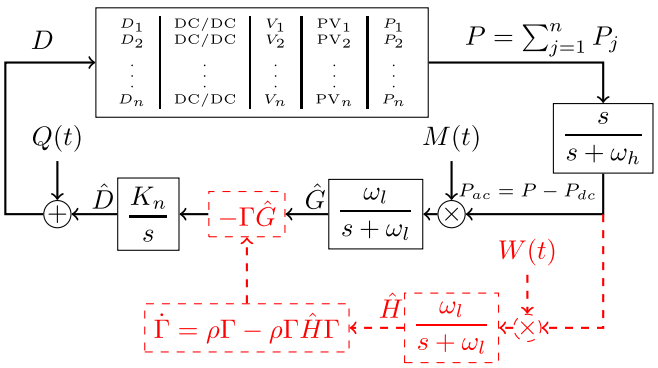

Fig. 6. Multivariable Newton-based ES for MPPT of a PV system. The red dashed part is added to the gradient-based ES to estimate the Hessian.

where the elements of $WQ^T H\tilde{D}$ are of the order of $1/a$ and have the harmonics of ω_j, $\omega_j \pm \omega_k \pm \omega_m$, and $2\omega_j \pm \omega_k$ for all distinct values of j, k, and m. The first term, $WQ^T HQ/2$, generates a dc value equal to the Hessian, H, with oscillatory parts of the order of $O(1)$, which can be neglected in comparison with the parts of the order of $O(1/a)$. It is critical to remove the harmonics of the order of $O(1/a)$ from the initial estimate of the Hessian, $W(t)P_{\rm ac}$. For this purpose, the low-pass filter should be designed with respect to the lowest harmonic of ω_j, $\omega_j - \omega_k - \omega_m$, and $2\omega_j - \omega_k$ for all distinct j, k, and m. As before (in the gradient-based design), this motivates the following restriction on the design of the low-pass filter frequency:

$$\omega_l \ll \min\left\{\omega_j, |\omega_j - \omega_k|, |\omega_j - \omega_k - \omega_m|, |2\omega_j - \omega_k|\right\} \tag{38}$$

for all distinct j, k, and m.

The goal of the Newton-based design is to replace the estimation error dynamics $\dot{\tilde{D}} = K_g H\tilde{D}$ with one of the form $\dot{\tilde{D}} = -K_n \Gamma H\tilde{D}$, where $\Gamma = H^{-1}$, that removes the dependence on the Hessian H. Calculating Γ, the estimate of the H^{-1}, in an algebraic fashion creates difficulties when $\hat{H}$ is close to singularity, or is indefinite. To deal with this problem, a dynamic estimator is employed to calculate the inverse of $\hat{H}$ using a Riccati equation.

Consider the following filter:

$$\dot{\mathcal{H}} = -\rho\mathcal{H} + \rho\hat{H}, \quad \rho = \omega\delta\rho'. \tag{39}$$

Note that the state of this filter converges to $\hat{H}$, an estimate of H. Denote $\Gamma = \mathcal{H}^{-1}$. Since $\dot{\Gamma} = -\Gamma\dot{\mathcal{H}}\Gamma$, then (39) is transformed to the differential Riccati equation

$$\dot{\Gamma} = \rho\Gamma - \rho\Gamma\hat{H}\Gamma. \tag{40}$$

The equilibria of the Riccati equation (40) are $\Gamma^* = 0_{n\times n}$ and $\Gamma^* = \hat{H}^{-1}$, provided $\hat{H}$ settles to a constant. Since $\rho > 0$, the equilibrium $\Gamma^* = 0$ is unstable, whereas the linearization of (40) around $\Gamma^* = \hat{H}^{-1}$ has the Jacobian $-\rho I_{n\times n}$, so the equilibrium at $\Gamma^* = \hat{H}^{-1}$ is locally exponentially stable. This shows that, after a transient, the Riccati equation converges to the actual value of the inverse of Hessian matrix if $\hat{H}$ is a good estimate of H.

Linearization of the update law for the error variable $\tilde{D} = \hat{D} - D^*$ results in

$$\dot{\tilde{D}} = -K_n \tilde{D}, \qquad K_n = \omega\delta\kappa_n > 0 \tag{41}$$

where elements of κ_n are $O(1)$ positive real numbers. According to (41), the convergence rate of the parameter is independent of the shape of the cost function, and therefore, after transient, when the Hessian is close enough to its actual value, the output power converges to the MPP with the same performance regardless of environmental or mismatch conditions. The analytical results in [6] can be rephrased as follows.

Theorem 2: For the system in Fig. 6, under Assumption 1, there exist $\bar{\delta}, \bar{a} > 0$ and for any $|a| \in (0, \bar{a})$ and $\delta \in (0, \bar{\delta})$, there exists $\bar{\omega} > 0$ such that for any given a and δ and any $\omega \in (0, \bar{\omega})$, there exists a neighborhood of the point $(\hat{D}, \hat{G}, \Gamma, \hat{H}, P_{\rm dc}) = (D^*, 0, H^{-1}, H, P(D^*))$ such that any solution of the Newton-based ES from the neighborhood exponentially converges to an $O(\omega+\delta+|a|)$ neighborhood of that point. Furthermore, $P(D, t)$ converges to an $O(\omega+\delta+|a|)$ neighborhood of $P(D^*)$.

V. Simulation and Experimental Results

To show the effectiveness of the proposed Newton-based design in Fig. 6, and compare its performance with that of the gradient-based design in Fig. 5, we present both simulation as well as experimental results for a PV system with $n = 2$ cascade modules. Before we present our results, some remarks on parameter selection, which has an important role in the performance of the multivariable design, are in order.

1) We select the probing frequencies small enough in comparison with the PWM frequency. We suggest that these be of the order of 1%–2% of the PWM frequency.
2) In the gradient-based case, the choice of the matrix gain K_g is more involved than the choice of K_n in the Newton-based design if one considers transient performance, and needs to be chosen with respect to the probing frequencies. In particular, higher gains are required for higher probing frequencies for the convergence rates to be more uniform as in the Newton-based approach. More details on this topic can be found in [9].
3) The transient for the estimate of the gradient vector contains frequencies that include harmonics of $\omega_i - \omega_j$, for all distinct i and j. The bandwidth of the low-pass filter needs to be designed with respect to these values.
4) We concluded from (37) that the raw estimate of the Hessian, $W(t)P_{\rm ac}$, has harmonics of the order of $1/a$ that should be attenuated by proper selection of ω_l, which reduces the fluctuation in the estimate of the Hessian, $\hat{H}$. We suggest selecting ω_l to be of the order of 5% of the least difference of harmonics in (38).
5) The final step is selecting the cutoff frequency of the high-pass filter, which we simply choose to be smaller than ω_l.

A. Simulation Results

For the simulations, the PV modules we use are model 215N from Sanyo, with datasheet parameters presented in Section II.

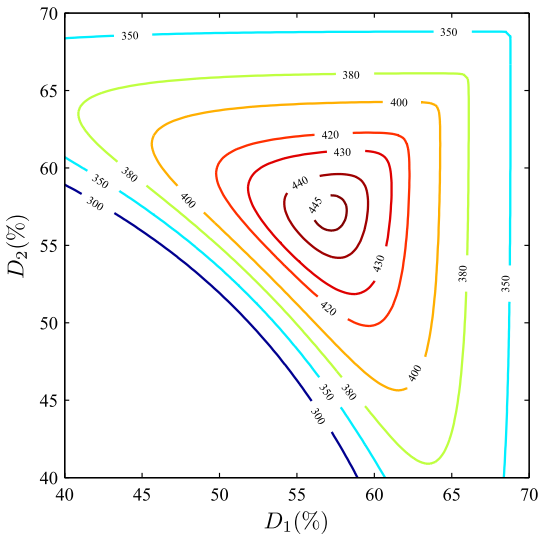

Fig. 7. Variation of the power of a cascade PV system including two Sanyo PV modules versus pulse duration, $D = [D_1 \;\; D_2]^T$. Level sets show the power in watt. $S_1 = S_2 = 1000$ W/m^2, $T_1 = T_2 = 25$ °C, and $V_{\rm dc} = 200$ V.

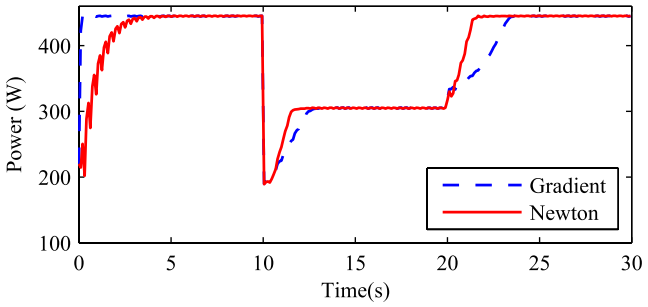

Fig. 8. Generated power in a partial shading scenario. Newton-based ES governs the system to its MPP with a uniform transient less than 5 s.

The variation of the generated power of a PV system including two series module from Sanyo connected to a dc bus with $V_{\rm dc} = 200$ V under standard test condition, $S = 1000$ W/m^2 and $T = 25$ °C, is shown in Fig. 7. MPP happens at $D = [\%57 \;\; \%57]^T$.

With the remarks for parameter selection, the numerical values of the design parameters are: $\omega_1 = 5000$ rad/s, $\omega_2 = 6000$ rad/s, $a = 0.01$, $\omega_l = 10$ rad/s, $\omega_h = 7$ rad/s, $H_0 = -10^5 \text{diag}([1 \;\; 1])$, $D_0 = [0.5 \;\; 0.5]^T$, $\rho = 10$, and $K_n = \text{diag}([1 \;\; 1])$. To make a fair comparison between gradient-based algorithm and Newton scheme, K_g should be of the order of $K_n\Gamma_0$, where $\Gamma_0 = H_0^{-1}$. However, we select $K_g = -30K_n\Gamma_0$ to make the comparison more strict for the Newton algorithm. The temperature T is assumed to be equal to 25 °C for all modules throughout. The irradiance S is assumed to be equal to 1000 W/m^2 initially, with a step change to 400 W/m^2 for modules PV_2 at $t = 10$ s and then back to 1000 W/m^2 at 20 s, so as to simulate partial shading. Modulation frequency of the PWM is $f_c = 100$ kHz.

Fig. 8 shows the output power of the entire system, and the estimates $\hat{D}$ and $\hat{H}$ of the pulse duration and Hessian, respectively, are shown in Figs. 9 and 10. It is clear from Fig. 8 that after the initial transient (roughly the first 5 s),

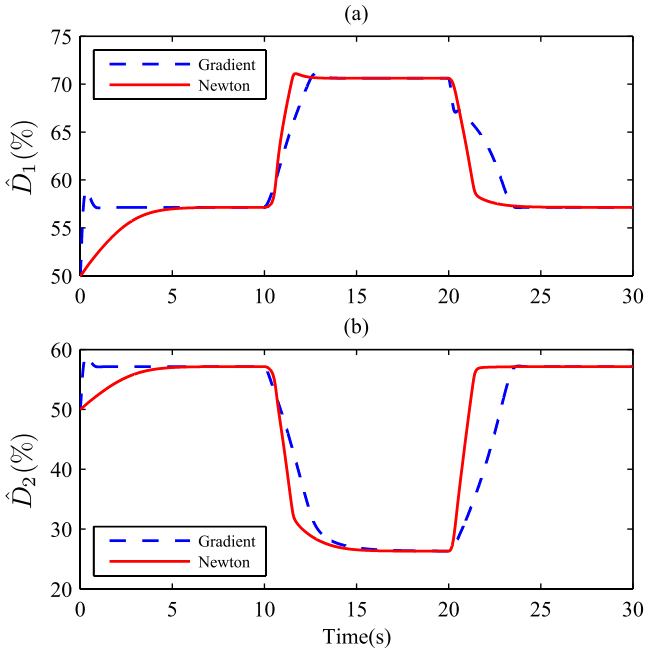

Fig. 9. Adaptation of the pulse duration for (a) converter 1 and (b) converter 2. Newton-based ES shows a similar convergence rate for all parameters. The convergence rate of the gradient-based ES varies with power level and direction of its variation.

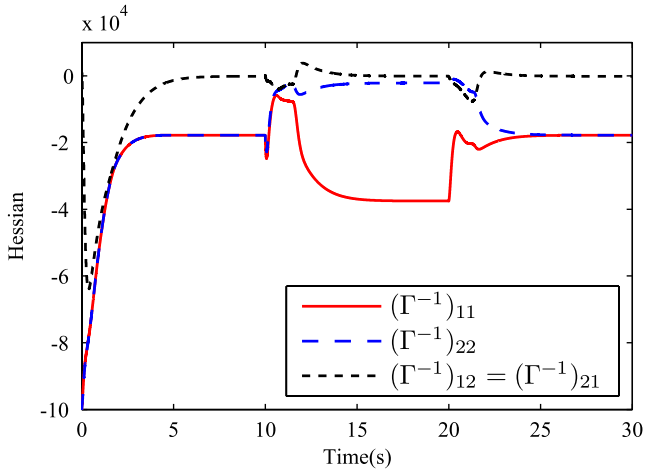

Fig. 10. Hessian matrix converges to its actual value.

the Newton-based algorithm performs a uniform and faster transient against step down (at 10 s) or step up (at 20 s) changes in the generated power. The transient of the gradient-based ES for all parameters is slightly faster than the Newton at the beginning, as shown in Fig. 9, resulting in the faster transient performance initially. Note that, at the beginning of the adaptation process, the estimate of Γ^{-1} is far from its actual value, which affects the transient convergence rate. However, the transient behavior of the Newton-based ES is more uniform in response to sudden changes in power level, while the gradient-based ES has different convergence rates for every parameter, which varies with the power level.

B. Experimental Results

Our hardware setup consists of two cascade PV modules connected to an active load, which plays the role of

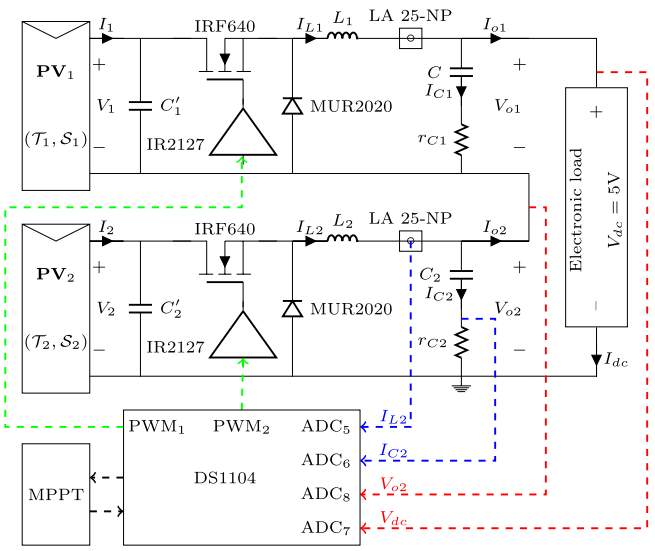

Fig. 11. Schematic view of the hardware setup.

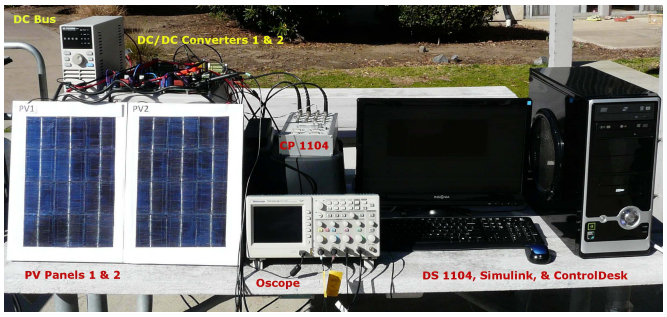

Fig. 12. Experimental setup.

the dc bus with $V_{\rm dc} = 5$ V, and is schematically shown in Fig. 11.

The physical hardware setup is shown in Fig. 12, and comprises of: 1) custom-made PV modules constructed using 12 PV cells; 2) power-pole boards developed by the University of Minnesota configured as dc/dc buck converters; and 3) DS1104 research and development controller board to implement our MPPT algorithms inside Simulink and interact with the dc/dc converters, and generate external PWM signals used by the dc/dc converters. Each power-pole board has a current sensor LA 25-NP to measure the inductor current, which we use along with the capacitor ripple current measurement to calculate the dc bus current. We employ the dc bus current and voltage to measure the power supplied to the dc bus.

The numerical values of the parameters are as follows: $\omega = 100\pi$ rad/s, $\omega_1 = 0.9\omega$, $\omega_2 = \omega, \omega_l = \omega_h = \omega/20, k_g = 2.5 \times 10^{-3}, K_g = k_g I_{2\times 2}, K_n = 0.08 I_{2\times 2}, H_0 = -400 I_{2\times 2}, a = 0.05$, and $D_0 = [\%70 \quad \%70]^T$. We use high-order Bessel filters instead of the first-order low- and high-pass filters to separate the ac and dc parts of the power signals and to create a smooth estimate of the gradient vector and the Hessain matrix. The PWM frequency is 100 kHz and the sampling time of the MPPT algorithm is 0.3 ms. The temperature of PV modules is 25 °C and the modules are fully exposed to the sun between 0–60 and 120–180 s.

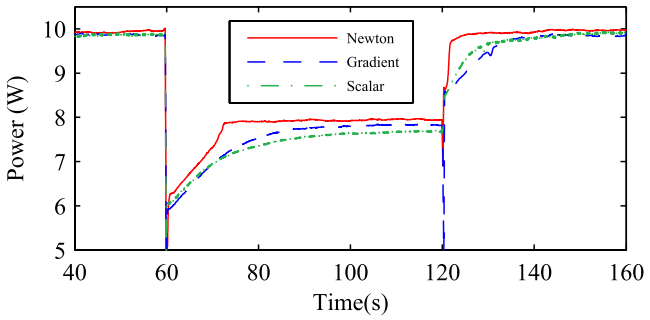

Fig. 13. Variation of power versus time. Newton algorithm shows uniform and fast transient with low steady-state error.

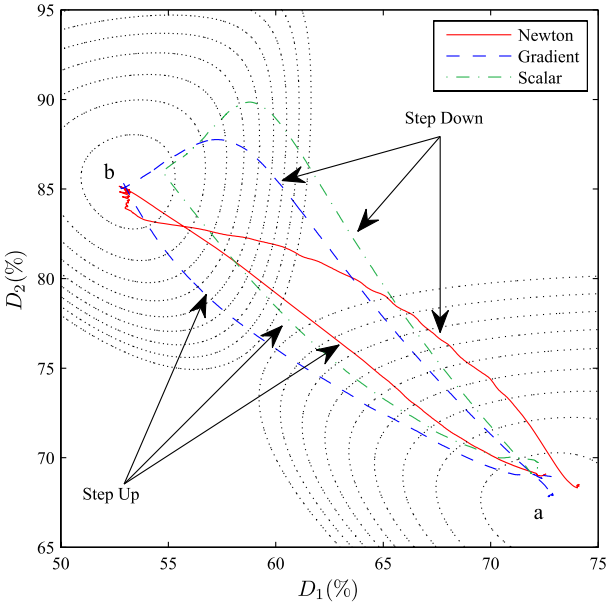

Fig. 14. Phase portrait of the MPPT for the multivariable Newton, multivariable gradient, and scalar gradient algorithms. Region shows (a) MPP area for full exposure to the sun and region (b) MPP area when PV_1 is partially shaded.

To simulate the effect of partial shading, PV_1 is covered with a plastic mat from time 60–120 s. When one module is partially shaded, the overall power level decreases. We not only compare the multivariable gradient- and Newton-based designs, but also the traditional scalar gradient-based design that has one MPPT loop for each converter.

Fig. 13 shows the performance of the three designs, and it is clear that the Newton algorithm recovers from this power level change faster than the other two algorithms. While the Newton method has the least steady-state error and uniform response under step-down and step-up power scenarios, the scalar design has the highest steady-state error and large response time in face of power decrease. The multivariable gradient-based ES performs better than the scalar MPPT under partial shading conditions.

The irradiance level of the partially shaded module is returned to normal level at $t = 120$ s. At this point, the Newton scheme shows faster transient in comparison with the similar transient of the multivariable gradient-based ES and the distributed ES. The results demonstrate that the convergence rate of the Newton scheme does not vary largely from step up to step down in power generation, which is not true for the gradient-based and distributed MPPT schemes. Not surprisingly, the experimental results are in keeping with the analytical and simulation results. Finally, as mentioned in Section IV, the Newton-based design moves the system in almost a straight line between extrema, in contrast to the curved steepest descent trajectories of the gradient algorithm. This observation is shown clearly in Fig. 14.

VI. Conclusion

Using ES in a microconverter configuration is a promising way to extract maximum power from a PV system. Conventionally used scalar gradient-based designs do so based on the generated power of each module. On the one hand, this requires two sensors per module, and on the other hand, the dependence on the level and direction of changes of the individual powers causes different transients in the parameter updates, particularly in response to sudden irradiance changes caused by partial shading. The multivariable gradient-based ES design removes some of these drawbacks. However, its performance still depends on the shape and curvature of the cost function that vary with environmental conditions. Since the Hessian of the entire system (and not individual modules) defines the performance of the parameter update, we can use the estimate of the Hessian to eliminate the dependence of the ES algorithm on environmental conditions that the Hessian depends upon. The Newton-based algorithm that we have presented does so, resulting in more uniform transients in response to irradiance and temperature changes, and improved the overall performance. The scheme also only uses two sensors for the overall system, resulting in lower hardware cost. The dual advantages contribute toward reduced average cost/watt, enhancing the economic viability of solar.

References

[1] K. Ariyur and M. Krstić, *Real-Time Optimization by Extremum Seeking Feedback*. New York, NY, USA: Wiley, 2003.

[2] A. Bratcu, I. Munteanu, S. Bacha, D. Picault, and B. Raison, "Cascaded DC-DC converter photovoltaic systems: Power optimization issues," *IEEE Trans. Ind. Electron.*, vol. 58, no. 2, pp. 403–411, Feb. 2011.

[3] S. Brunton, C. Rowley, S. Kulkarni, and C. Clarkson, "Maximum power point tracking for photovoltaic optimization using ripple-based extremum seeking control," *IEEE Trans. Power Electron.*, vol. 25, no. 10, pp. 2531–2540, Oct. 2010.

[4] S. Dhople, J. Ehlmann, A. Davoudi, and P. Chapman, "Multiple-input boost converter to minimize power losses due to partial shading in photovoltaic modules," in *Proc. IEEE ECCE*, Sep. 2010, pp. 2633–2636.

[5] T. Esram and P. Chapman, "Comparison of photovoltaic array maximum power point tracking techniques," *IEEE Trans. Energy Convers.*, vol. 22, no. 2, pp. 439–449, Jun. 2007.

[6] A. Ghaffari, M. Krstić, and D. Nešić, "Multivariable Newton–based extremum seeking," *Automatica*, vol. 48, no. 8, pp. 1759–1767, 2012.

[7] A. Ghaffari, M. Krstić, and S. Seshagiri, "Power optimization for photovoltaic micro-converters using multivariable Newton–based extremum-seeking," in *Proc. Conf. Decision Control*, 2012, pp. 2421–2426.

[8] A. Ghaffari, S. Seshagiri, and M. Krstíc, "High-fidelity PV array modeling for advanced MPPT design," presented at the IEEE CCECE, Montreal, QC, Canada, Apr. 2012.

[9] A. Ghaffari, S. Seshagiri, and M. Krstić, "Power optimization for photovoltaic micro-converters using multivariable gradient-based extremum-seeking," in *Proc. Amer. Control Conf.*, Jun. 2012, pp. 3383–3388.

[10] A. Ghaffari, S. Seshagiri, and M. Krstić, "Power optimization for photovoltaic micro-converters using multivariable gradient-based extremum-seeking," *Control Eng. Practice*, to be published.

[11] D. P. Hohm and M. E. Ropp, "Comparative study of maximum power point tracking algorithms," *Progr. Photovolt., Res. Appl.*, vol. 11, no. 1, pp. 47–62, 2003.
[12] S. Jain and V. Agarwal, "Comparison of the performance of maximum power point tracking schemes applied to single-stage grid-connected photovoltaic systems," *IET Electr. Power Appl.*, vol. 1, no. 5, pp. 753–762, Sep. 2007.
[13] M. Krstić and H.-H. Wang, "Stability of extremum seeking feedback for general nonlinear dynamic systems," *Automatica*, vol. 36, no. 4, pp. 595–601, 2000.
[14] P. Lei, Y. Li, Q. Chen, and J. Seem, "Extremum seeking control based integration of MPPT and degradation detection for photovoltaic arrays," in *Proc. Amer. Control Conf.*, Jul. 2010, pp. 3536–3541.
[15] M. Miyatake, M. Veerachary, F. Toriumi, N. Fuji, and H. Ko, "Maximum power point tracking of multiple photovoltaic arrays: A PSO approach," *IEEE Trans. Aerosp. Electron. Syst.*, vol. 47, no. 1, pp. 367–380, Jan. 2011.
[16] S. Moura and Y. Chang, "Asymptotic convergence through Lyapunov-based switching in extremum seeking with application to photovoltaic systems," in *Proc. Amer. Control Conf.*, Jul. 2010, pp. 3542–3548.
[17] F.-S. Pai, R.-M. Chao, S. H. Ko, and T.-S. Lee, "Performance evaluation of parabolic prediction to maximum power point tracking for PV array," *IEEE Trans. Sustain. Energy*, vol. 2, no. 1, pp. 60–68, Jan. 2011.
[18] G. Petrone, G. Spagnuolo, and M. Vitelli, "A multivariable perturb-and-observe maximum power point tracking technique applied to a single-stage photovoltaic inverter," *IEEE Trans. Ind. Electron.*, vol. 58, no. 1, pp. 76–84, Nov. 2011.
[19] C. A. Ramos-Paja, G. Spagnuolo, G. Petrone, M. Vitelli, and J. Bastidas, "A multivariable MPPT algorithm for granular control of photovoltaic systems," in *Proc. IEEE Int. Symp. Ind. Electron.*, Jul. 2010, pp. 3433–3437.
[20] G. Vachtsevanos and K. Kalaitzakis, "A hybrid photovoltaic simulator for utility interactive studies," *IEEE Trans. Energy Convers.*, vol. EC-2, no. 2, pp. 227–231, Jun. 1987.

Azad Ghaffari received the B.S. degree in electrical engineering and the M.S. degree in control engineering from the K. N. Toosi University of Technology, Tehran, Iran, and the Ph.D. degree in mechanical and aerospace engineering from the Joint Doctoral Program between San Diego State University and the University of California, San Diego, CA, USA.

His current research interests include demand response in power systems, extremum seeking, and its application to maximum power point tracking in the photovoltaic and wind energy conversion systems, induction machines, power electronics, and sliding mode control.

Miroslav Krstić (F'01) received the Ph.D. degree in electrical engineering from the University of California, Santa Barbara, CA, USA, in 1994.

He was a Daniel L. Alspach Endowed Chair and is the Founding Director of the Cymer Center for Control Systems and Dynamics, University of California, San Diego, CA, USA. He serves as an Associate Vice Chancellor for Research with the University of California. He has co-authored ten books on adaptive, nonlinear, and stochastic control, extremum seeking, control of PDE systems, including turbulent flows and control of delay systems.

Dr. Krstić is a fellow of IFAC. He is a recipient of the PECASE, NSF Career, and ONR Young Investigator Awards, as well as the Axelby and Schuck Paper Prizes, and was the first recipient of the UCSD Research Award in engineering. He has held the Russell Severance Springer Distinguished Visiting Professorship at UC Berkeley and the Royal Academy of Engineering Distinguished Visiting Professorship. He serves as a Senior Editor for the IEEE TRANSACTIONS ON AUTOMATIC CONTROL and *Automatica*, an Editor of two Springer book series, and has served the Vice President for technical activities of the IEEE Control Systems Society and a Chair of the IEEE CSS Fellow Committee.

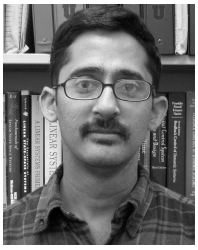

Sridhar Seshagiri received the B.Tech., M.S., and Ph.D. degrees in electrical engineering from IIT Madras, Chennai, India, and Michigan State University, East Lansing, MI, USA, in 1995, 1998, and 2003, respectively.

He was with the Department of Electrical and Computer Engineering, San Diego State University, San Diego, CA, USA, in 2003, where he is currently an Associate Professor. His current research interests include nonlinear control with applications to energy systems, particularly control of power electronic converters.